Towards narrowing uncertainty in future projections of local extreme precipitation

Francesco Marra[1], Moshe Armon[2], Ori Adam[3], Davide Zoccatelli[4], Osama Moh'd Najeeb Gazal[5], Chaim I Garfinkel[2], Dorita Rostkier-Edelstein[6], Uri Dayan[7], Yehouda Enzel[2], and Efrat Morin[8]

[1]Institute of Atmospheric Sciences and Climate, National Research Council
[2]Hebrew University of Jerusalem
[3]Hebrew University
[4]University of Padova
[5]Faculty of Agricultural and Environmental Sciences, Szent Istvan University
[6]Department of Environmental Physics, Environmental Sciences Division, IIBR
[7]Department of Geography, Hebrew University of Jerusalem
[8]Institute of Earth Sciences, The Hebrew University of Jerusalem

November 28, 2022

Abstract

Projections of extreme precipitation based on modern climate models suffer from large uncertainties. Specifically, unresolved physics and natural variability limit the ability of climate models to provide actionable information on impacts and risks at the regional, watershed and city scales relevant for practical applications. Here we show that the interaction of precipitating systems with local features can constrain the statistical description of extreme precipitation. These observational constraints can be used to project local extremes of low yearly exceedance probability (e.g., 100-year events) using synoptic-scale information from climate models, which is generally represented more accurately than the local-scales, and without requiring climate models to explicitly resolve extremes. The novel approach offers a path for improving the predictability of local statistics of extremes in a changing climate, independent of pending improvements in climate models at regional and local scales.

Towards narrowing uncertainty in future projections of local extreme precipitation

Francesco Marra[1,2,*], Moshe Armon[1], Ori Adam[1], Davide Zoccatelli[1], Osama Gazal[3], Chaim I. Garfinkel[1], Dorita Rostkier-Edelstein[1,4], Uri Dayan[5], Yehouda Enzel[1], and Efrat Morin[1]

[1]The Fredy and Nadine Herrmann Institute of Earth Sciences, The Hebrew University of Jerusalem, Israel

[2]Institute of Atmospheric Sciences and Climate, National Research Council of Italy, CNR-ISAC, Bologna, Italy

[3]Faculty of Agricultural and Environmental Sciences, Szent Istvan University, Hungary

[4]Department of Environmental Physics, Environmental Sciences Division, IIBR, Ness-Ziona, Israel

[5]Department of Geography, The Hebrew University of Jerusalem, Israel

Corresponding author: Francesco Marra (f.marra@isac.cnr.it)

*Via Gobetti, 101, 40129, Bologna, Italy

Key Points:

- Local observations can be used to constrain the intensity distribution of precipitation events associated to different synoptic systems
- The constraints allow projecting extreme return levels at scales relevant for impact studies from synoptic information from climate models
- The approach improves the predictability of local extremes, independent of improvements in climate models at regional and local scales

Abstract

Projections of extreme precipitation based on modern climate models suffer from large uncertainties. Specifically, unresolved physics and natural variability limit the ability of climate models to provide actionable information on impacts and risks at the regional, watershed and city scales relevant for practical applications. Here we show that the interaction of precipitating systems with local features can constrain the statistical description of extreme precipitation. These observational constraints can be used to project local extremes of low yearly exceedance probability (e.g., 100-year events) using synoptic-scale information from climate models, which is generally represented more accurately than the local-scales, and without requiring climate models to explicitly resolve extremes. The novel approach offers a path for improving the predictability of local statistics of extremes in a changing climate, independent of pending improvements in climate models at regional and local scales.

Plain Language Summary

Climate change impact studies are currently restrained by the limited accuracy of climate models in resolving precipitation extremes and by the uncertainties characterizing their analysis. We use here a novel approach which permits to project extreme precipitation for future climatic scenarios based on the combination of coarse-scale information from climate models with local observations. Focusing on the south-eastern Mediterranean, we provide projections of precipitation extremes which could not yet be derived using traditional methods, such as the events occurring on average once in 100 years. The combined effect of changes in intensity and average yearly number of two dominant synoptic systems is projected to increase the intensity of the 100-year events in the coast and in the desert areas of the region, and to decrease it elsewhere. The novel approach offers a path for improving the predictability of extremes in a changing climate, independent of pending improvements in climate models.

1 Introduction

In recent decades, natural hazards associated with extreme precipitation, such as floods and landslides, claimed thousands of lives and billions of US$ in damages every year (NOAA, 2020; Paprotny et al., 2018). These numbers are expected to grow in response to an expansion of population and wealth towards hazard-prone areas and to modifications in the hydrological cycle induced by climate change (Ceola et al., 2014; Fischer and Knutti, 2016; Winsemius et al., 2016). Quantifying climate change impact on extremes is thus a major challenge for the research community (Blöschl et al, 2019). Hydrological design and risk management, particularly relevant for adaptation efforts, require information on low *yearly* exceedance probabilities (Chow et al., 1988), such as the events exceeded on average once in 100 years (hereon 100-year *return levels*, with 1% yearly exceedance probability). To directly quantify return levels, long data series are required, several times longer than the exceedance probability timescale. Since observational records rarely exceed 50-100 years, some form of statistical extrapolation is generally required (Coles, 2001).

Earth system models (ESMs) are commonly used to guide impact studies. However, current ESMs are not able to explicitly resolve convective and microphysical processes critical for precipitation extremes, and rely instead on parameterizations (Wilcox and Donner, 2007). Additionally, their output is most relevant at scales which are too coarse for many practical applications (Fischer et al., 2013; Hausfather et al., 2019). Dynamical downscaling methods can provide projections for a region of interest, but are sensitive to the boundary conditions provided by global models (Shepherd, 2014; Keller et al., 2018). Furthermore, their application is limited by computational requirements so that, currently, only few regions are covered with 10-20-year simulations (Kendon et al., 2014; Fosser et al., 2020), which are too short to reliably estimate 10-years return levels, let alone 100-year events. Alternatively, statistical models are combined with variables that are strongly related to extreme precipitation but more reliably reproduced in ESMs, such as temperature (Snippel et al, 2015; Pfahl et al., 2017).

The methods currently adopted to quantify return levels, however, heavily rely on extremes, such as the maxima values in each year or the values exceeding high thresholds (Coles, 2001). As these are rare and subject to large uncertainties, the applicability of these methods in a changing climate is limited (Serinaldi and Kilsby, 2015). In fact, stochastic climate variability sets a lower bound on the uncertainty in observed and modelled extremes (Fatichi et al., 2016). Reliable projections of extreme return levels for future climate scenarios thus necessarily entail either intensive dynamical downscaling of ESMs with convection-permitting models, or novel statistical approaches able to better exploit the available information.

It is shown here that the interaction of precipitating systems with local features, such as coastlines or orography, can constrain the statistical description of precipitation intensity. These constraints, derived from in-situ observations, permit predicting future extreme return levels at the local-scales based on coarse-resolution global climate model projections, and without requiring models to explicitly resolve the extremes.

2 Study area and data

The south-eastern Mediterranean is regarded as a climate change hotspot, highly vulnerable to water scarcity and precipitation-induced hazards (Alpert et al., 2002; Giorgi, 2006). Strong spatial gradients in precipitation climatology (Fig. S1 and S2 in the Supporting Information) emerge from the interactions of two main types of precipitating systems with coastline and orography (Diskin, 1970): (i) low-pressure systems moving inland along westerly tracks (Mediterranean cyclones, hereon *Type-1*), and (ii) low-pressure systems mainly extending from the south (active Red Sea troughs, *Type-2*). These are characterized by distinct spatial patterns and both yield extreme precipitation amounts (Armon et al., 2018; Marra et al., 2019a). ESMs predict substantial changes in the intensity and occurrence frequency of both systems

(Hochman et al., 2018a; Hochman et al., 2018b; Zappa et al., 2015), implying non-linear changes in the compound extremes, which can be further complicated by local effects.

2.1 Precipitation data

Daily precipitation data, summed up to 6:00UTC, were provided by the Ministry of Water and Irrigation of Jordan (97 stations between 1980-1981 and 2017-2018) and the Israel Meteorological Service (>1300 stations between 1948-1949 and 2017-2018). Data from Israeli stations flagged as missing, inaccurate, interpolated or obtained from multi-day accumulations were excluded from the analysis. Jordanian data were supplied with no quality indicators; we therefore rely on quality controls by the data provider. Separate records measured in proximity of up to 1 km distance and 50 m elevation were merged. Records were organized by hydrologic years (September 1 to August 31). For each station, years with more than 14 unavailable days and records with less than 30 hydrological years were discarded. The final dataset consists of 459 stations (404 from Israel, 55 from Jordan, average spatial density of ~1/75 km^{-2}) with 30-70 complete years of record (50.1±13.3 years). Stationarity of the annual maxima at each station is ensured using the Phillips and Perron (1988) test (5% significance level), indicating that the data adequately represent extremes under present conditions.

2.2 Local groups of stations

Groups of stations in which distinct local features dominate the interaction with the precipitating systems are identified using a *kmeans* clustering algorithm based on geographical (latitude, longitude, elevation) and precipitation (average wet-day amount, and standard deviation of the wet-day amounts) properties, without any direct use of extreme precipitation properties or classification of the precipitating systems. The variables are normalized to zero-mean equi-dispersed distributions; the algorithm is iterated 99 times to ensure stable results. Following the Calinski and Harabasz (1974) criterion, six groups are obtained, roughly identifiable as: mountains, northern coast, lowlands, coast, deserts west of the Dead Sea rift, and deserts east of the rift. The last two groups are characterized by similar climatic conditions and are likely separated primarily due to the geographical distance, although differences in other aspects may exist, such as elevation and distance from the sea. These two groups, which are sparsely populated (only 21 stations in one group), were merged. The classification used in the analysis consists of five groups: mountains, northern coast, lowlands, coast, and deserts (Fig. 1a).

3 Methods

Extreme precipitation events were shown to emerge from underlying distributions of ordinary events (Marani and Ignaccolo, 2015; Zorzetto et al., 2016), whose tails are generally described by two parameters (e.g., stretched-exponential or power-type) (Cavanaugh et al., 2015; Papalexiou et al., 2018; Marra et al., 2020b). By relying on ordinary events, for which more data is available, this approach decreases the stochastic uncertainties inherent in the realization of extremes (Zorzetto et al., 2016; Marra et al., 2018). Events generated by different types of processes and thus described by distinct distributions such as mid-latitude vs. tropical cyclones (or, in our case, *Type-1* vs. *Type-2*) can be combined to derive a compound distribution for extreme return levels (Marra et al., 2019a; Miniussi et al., 2020). This distribution quantifies the yearly exceedance probability ζ associated with the precipitation amount x as a function of the intensity distributions of the ordinary events ($F_{i=1,\dots,S}$, where i represents the type of process) and the expected value of their yearly number of occurrences (n_i) such that: $\zeta(x) \simeq F_1^{n_1} \cdot F_2^{n_2} \cdot \dots \cdot F_S^{ns}$ (Marra et al., 2019a). In this framework, changes in extreme return levels can be expressed as functions of the projected changes in the intensity distributions of the ordinary events and in the expected value of their yearly occurrences. While the occurrence frequency of synoptic events in the region can be resolved by ESMs (Hochman et al., 2018a; Cavicchia et al., 2020), precipitation intensity requires information on *two* degrees of freedom (i.e., the two parameters describing the distribution).

3.1 Ordinary events distributions and return levels

Ordinary events are defined as non-zero (i.e., ≥ 0.1 mm) daily precipitation amounts (Zorzetto et al., 2016) associated with a precipitation type based on a semi-automatic, daily-based, synoptic classification (Alpert et al., 2004). Wet days corresponding to systems that are expected to be dry may have been wrongly classified; for example, synoptic conditions in the aftermath of Mediterranean cyclones are easily misinterpreted by the semi-automatic method. These were individually examined and labelled as *Type-1* if occurring up to 2 days after a *Type-1* day, and as *Type-2* in the remaining cases (Table S1).

Previous studies show that a Weibull distribution (stretched-exponential) in the form $F(x; \lambda, \kappa) = 1 - e^{-\left(\frac{x}{\lambda}\right)^{\kappa}}$, where λ is the scale and κ the shape parameter, well describes the tail of the two types of ordinary events in the region (Marra et al., 2019a). The shape parameter determines the tail heaviness, with heavier tails for smaller shapes and vice versa. These parameters are estimated left-censoring the lowest 75% of the observations while keeping their weight in probability, and using a least-square linear regression in Weibull-transformed coordinates (Marra et al., 2019a). The left-censoring prevents contaminations from the lower tail of the distribution, which may require more general formulations (Papalexiou et al., 2018; Cavanaugh et al., 2015) and is sensitive to the accuracy of the measurement device (Marra et al., 2019a). After left-censoring, the number of data points used for the parameter estimation in each of the stations is 426 ± 175 for *Type-1* (minimum 66), and 153 ± 68 (minimum 30) for *Type-2*. The expected number of yearly ordinary events is computed, for each type, as the mean of the yearly number of wet days. Extreme return levels are computed numerically by inverting the formulation $\zeta(x) \simeq F_1^{n_1} \cdot F_2^{n_2}$. Sample uncertainty in parameters and return levels is quantified via bootstrap with replacement (10^3 repetitions) among the years in the record (Overeem et al., 2008). The resulting return levels (Fig. 1; Fig. S2) are consistent with traditional methods based on the observed annual maxima (Fig. S3), but have significantly smaller uncertainty (22%, as opposed to 39%, median uncertainty on 100-year return levels).

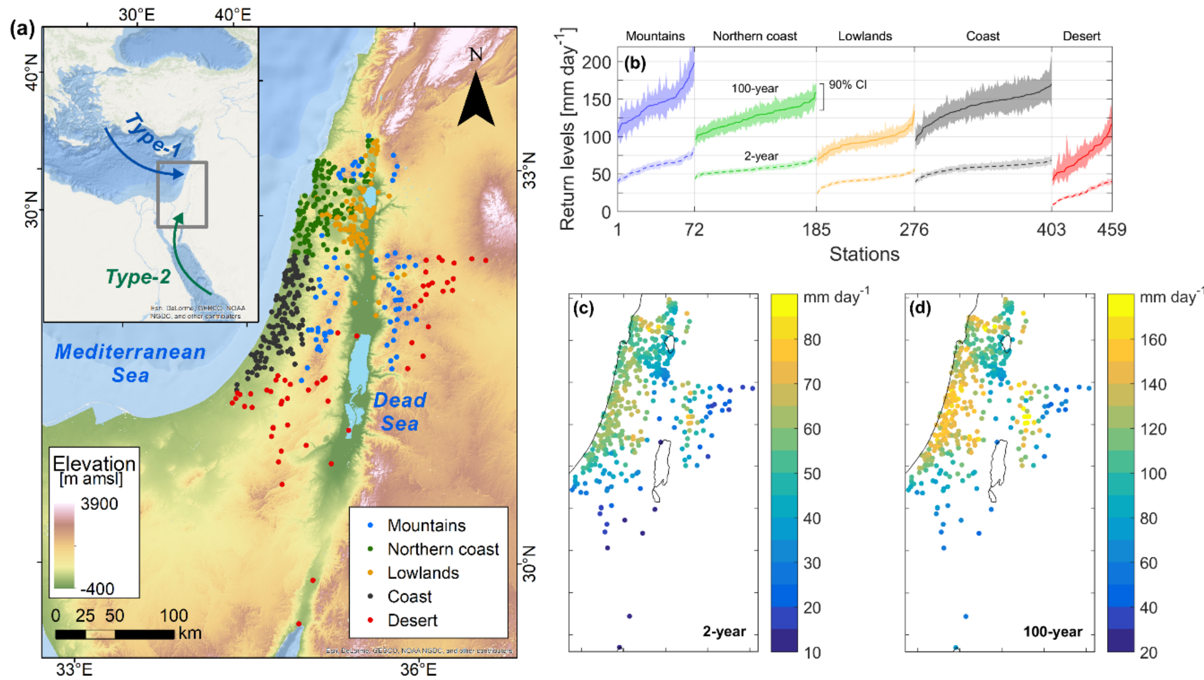

Figure 1. Extremes emerge from the interaction of precipitation systems with local features. (a) Map of the study region showing the local terrain elevation, the main precipitating systems tracks, and the location of the daily precipitation stations used in the study, coloured according to groups in which different local features dominate the interaction with the precipitating systems. (b) Distribution of 2-year and 100-year return levels (50% and 1% yearly exceedance probability, respectively) of the five groups shown in panel a (with matching colours) displayed as transposed cumulative distributions. The respective uncertainty (shading) is calculated as the 90% confidence interval from 10^3 bootstrap samples with replacement among the years in the record. The median uncertainty across all groups is 14% (22%) for 2-year (100-year) return levels. (c, d) Map of the 2-year (c) and 100-year (d) return levels (colours indicate daily precipitation intensity).

3.2 Local constraints of the intensity distributions

A robust relationship between the scale λ and shape κ parameter of the ordinary events distributions would reduce the representation of precipitation intensity to *one* degree of freedom, enabling us to provide projections of extremes based only on changes in the mean intensity of ordinary events. The significance of the relationship between the parameters describing the two types of ordinary events at each of the five groups of stations is tested using the rank correlation (10^4 Monte Carlo reshuffling realizations). The coefficient α of the relations in the form $\kappa = \alpha \cdot \log \lambda + C$ is derived for each of the five groups and the two event types using a linear regression model based on a χ^2 minimization and considering parameter estimation errors in a Monte Carlo framework (10^3 realizations).

The coefficients α, calculated for each group, represent the local constraints on the intensity distribution. Higher α implies a stronger decrease in tail heaviness in response to an increase in the median intensity, and vice versa. Under these constraints the distribution has one degree of freedom, meaning that any quantity not orthogonal to the constraint (e.g., mean, median, standard deviation, etc.) is sufficient to describe the distribution. Here, we use the median intensity, hereon denoted I, as it is less sensitive than the mean to the stochastic uncertainty in the realization of extremes: $F_i(x; \lambda_i, \kappa_i) = F(x; I_i)$. The return level x associated with the yearly exceedance probability p can be written as a function of median intensity and expected number of yearly occurrences of the two types of ordinary events by inverting the extreme value distribution $\zeta(x)$: $x(p) = \zeta^{(-1)}(p; I_1, n_1; I_2, n_2)$.

We assume that temporal changes in the distribution of ordinary events will preserve these local observational constraints. This resembles the assumptions behind regionalization approaches in which spatial information is traded for record length (Buishand, 1991), but extends its meaning in that (i) temporal changes are allowed, and (ii) the information on the interaction between precipitating systems and local features provided by each individual station is fully exploited (e.g. Marra et al., 2020a). To support our assumption, we test the significance of the constraints in historical observations in a Monte Carlo framework by examining groups of non-consecutive years with consistently different median intensity (see Fig. S4) along the following steps: (1) at each station and precipitation type, years are ranked according to the median ordinary events intensity; (2) six 5-year subsets of non-consecutive years are created by selecting three groups (15 years) from the largest intensity years and three from the smallest intensity; (3) Weibull parameters are estimated at each station for the 5-year subsets; (4) 10^3 m-elements synthetic samples, where m is the number of wet-days in the observed 5-year subsets, are generated according to the obtained distributions and the parameters describing the samples are estimated to quantify the impact of parameter estimation uncertainty; (5) logarithmic relations between the parameter pairs are derived for each subset; (6) the α coefficient representing the local constraint is compared to the distribution of coefficients of the logarithmic relations at (5).

3.3 Climate projections

Projected changes in median intensity and expected number of yearly occurrences of the two precipitation types are obtained by examining the difference between the ends of the 21st century (~2080-2100) and the 20th century (~1980-2005) under the RCP8.5 emission scenario (Riahi et al., 2011). We estimated these differences using the data presented in Hochman et al. (2018a) and Zappa et al. (2015), calculated for 8 and 17 CMIP5 models, respectively. We choose the changes in occurrence and median intensities from these two studies, as they are produced for the desired time period and emission scenario, and because these parameters are considered more robust than the changes in extremes that can be derived from the CMIP5 models themselves (Fatichi et al., 2016). In particular, the changes in synoptic circulation over the study region derived from CMIP5 ensembles were shown to be robust (Hochman et al., 2017; Hochman et al., 2018a; Zappa et al., 2015).

The acquired changes we used are: *Type-1*: expected number of yearly occurrence is projected to decrease by 15-35% (-25 ± 10 %); median intensity is projected to decrease by 20-25% ($+22.5 \pm 5$ %); *Type-2*: expected number of yearly occurrence is projected to increase by

13% ($+13 \pm 5$ %); annual *Type-2* precipitation amounts are projected to remain unchanged, which leads to a 12% decrease in the median intensity (-12 ± 5 %). These numbers result in a 20-30% decrease in mean annual precipitation, which is consistent with the AR5 IPCC report (IPCC, 2014). As based on relative differences between historic and future simulations, we expect these projections to be less sensitive to systematic biases in the quantification of wet days from CMIP5 models (e.g., too many drizzle days).

Changes in extreme return levels are computed in a Monte Carlo framework considering uncertainties in the projections and in the local constraints (i.e., the α coefficients), as follows. At each station, 10^3 projections are created by (1) sampling the projected change in number and median intensity of the two ordinary events types from normal distributions, and (2) sampling the α coefficient of the local constraint relations from the Monte Carlo realizations. Note that, since the ratio between median and mean of Weibull distributions smoothly depends on the shape parameter κ and is independent from the scale λ, one can safely assume a one-to-one correspondence between projected changes in the mean and in the median (e.g., a 5% change in the mean corresponds to ~5% change in the median). This is useful since the median is a better descriptor for observed data whereas the mean is commonly provided by ESMs output.

4 Application to the south-eastern Mediterranean

4.1 Local constraints on the distribution of ordinary events

While relations between scale λ and shape κ parameters of the ordinary events distributions are not expected *a priori*, statistically significant relations (>3σ significance level) are found for the given data when focusing on local groups of stations in which distinct local features dominate the interactions with precipitation systems (Fig. 2a-c; Fig. S4). Dependence of the form $\kappa = \alpha \cdot \log \lambda + C$, where α and C are empirically-determined, was found to approximate these relations in each group, generally explaining most of the observed variance (Fig. S4). The hypothesis of a local constraint α being significantly different from the coefficients obtained from temporally splitting the records is rejected in all the cases (5% significance level). Thus, the local values of α indeed reflect historical changes in the median intensity of ordinary events at each station, supporting the validity of the approach under changing conditions (Fig. 2c; Fig. S4). It is worth noting that these relations are based on historical observations and thus comprise observed changes in both dynamics and thermodynamics.

The observed constraints imply that changes in the median intensity are linked to contrasting changes in extremes, i.e., decreasing median intensity decreases the precipitation amount yielded by typical ordinary events (Fig. 2d, e) but increases the probability associated with the largest events, and *vice versa* (Fig. 2f). This counter-intuitive behaviour is consistent with previous theory and observations of extreme precipitation, and supports the local constraints approach as a framework for quantifying changes in extremes (O'Gormann and Schneider, 2009; Pendergrass, 2018; Pendergrass and Knutti, 2018; Myhre et al., 2019; Wasko et al., 2018).

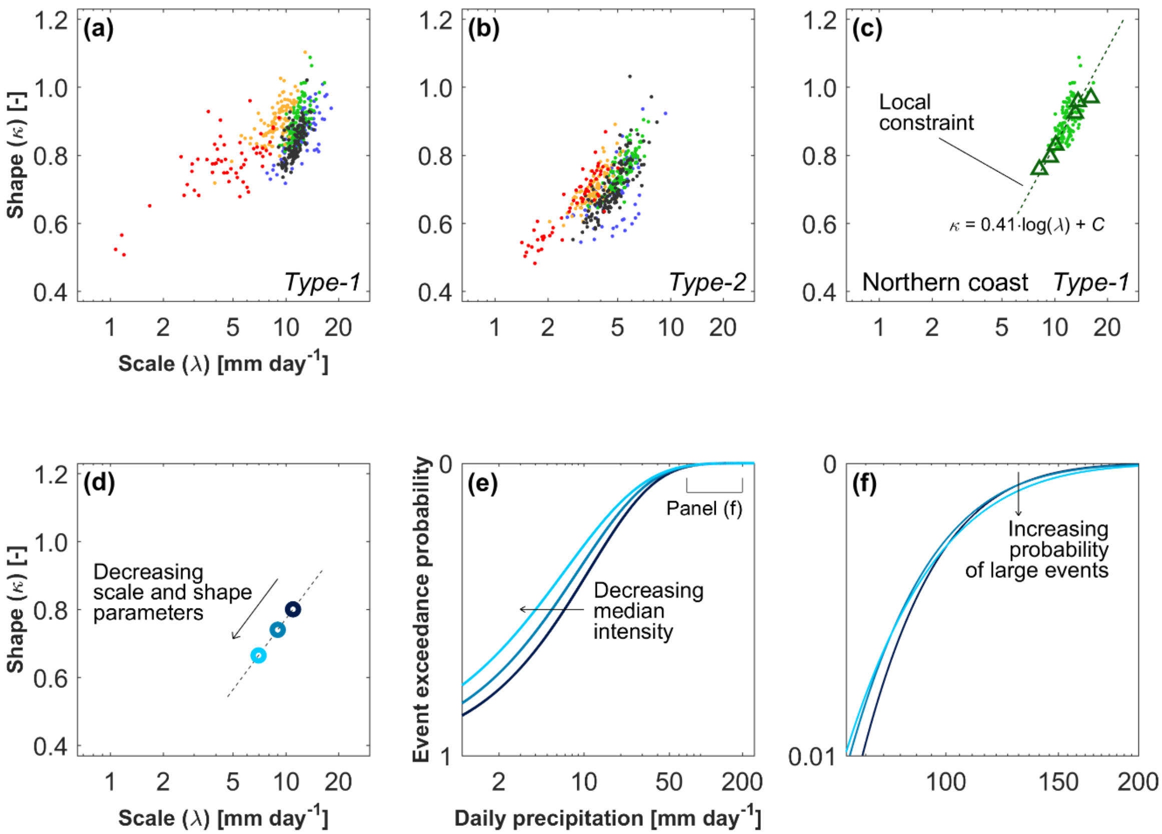

Figure 2. Local constraints on the intensity distribution of ordinary precipitating events. (a, b) Scatter plots of the shape (κ) and scale (λ) parameters of the observed distributions for the two types of ordinary events; colours refer to the five groups of stations as in Fig. 1a. (c) Example of the local constraint (*Type-1*, northern coast); triangles represent the median (among stations) parameters obtained in the split-sample test using, for each station, groups of five non-consecutive years with increasing median intensity of the ordinary events; triangles thus represent historical variations of intensity. Local constraints for all cases are shown in Fig. S4. (d) Schematic of the projection of changes in the intensity distribution of the ordinary events along the constraints ($\alpha = 0.3$, $\lambda = 11.0, 9.0, 7.0$ mm day^{-1} and $\kappa = 0.8, 0.74, 0.66$; black, blue and cyan, respectively); (e) event exceedance probability distributions associated with the three pairs of scale and shape parameters shown in (d); (f) the largest 1% of the events in these distributions.

4.2 Projections of future extremes

The sensitivity of extreme return levels to changes in the ordinary events (Fig. S5; Fig. S6) highlights that different return levels can have different responses, and that the local sensitivities associated with each event type can differ significantly. For example, in most of the region return levels are tied to changes in intensity and number of *Type-1* events, while changes in *Type-2* are crucial drivers for extreme return levels in the desert areas (Fig S5). Local changes in extreme return levels are thus related to mean (or median) changes in precipitation in a complex manner.

The projected changes in occurrence frequency of the two types (25% decrease and 13% increase, respectively) and intensity (20-25% and 12% decrease, respectively), yield the changes in the extreme return levels shown in Fig. 3 (see Fig. S7 for more details). An overall 5-20% decrease of the 2-year return levels is seen, driven by the decrease in the occurrence frequency of Mediterranean cyclones and in the median intensity of both types of systems. Since in the climatological setting of the region 2-year return levels roughly correspond to 99th wet-day percentiles, this is consistent with previous results based on downscaling methods (Hochman et al, 2018b). The picture is drastically different for the 100-year return levels which could not be assessed in previous studies. Along the coast and in the southern desert, the negative sensitivity to changes in the median intensity (Fig. S5; Fig. S6) dominates, and the rarest extremes are projected to increase, consistently with Fig 2f. These results imply two adverse effects: (i) amplified water scarcity and reduced flood and landslide risks in most of the region (Alpert et al., 2002; Samuels et al., 2009; Peleg et al., 2015); and (ii) increased intensity of the most severe events along the coast and southern deserts, associated with augmented risk of extreme pluvial flooding in coastal cities, and of flash floods, debris flows and geomorphic responses in the southern deserts (Shmilovitz et al., 2020; Rinat et al., 2020).

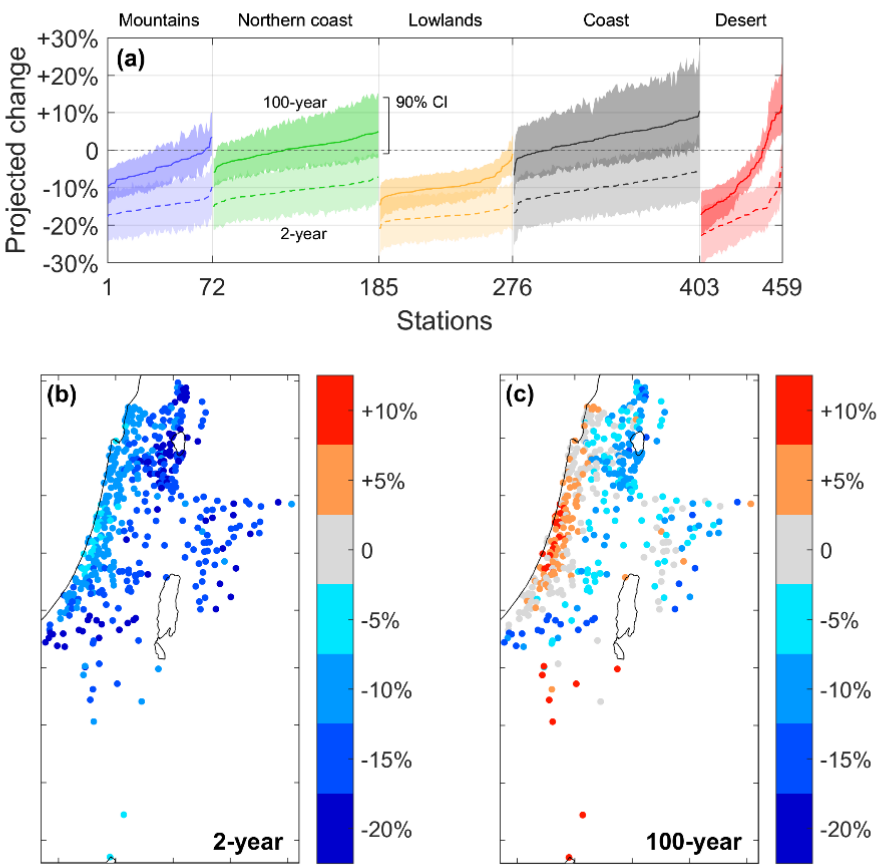

Figure 3. Projected changes in extreme precipitation return levels. Projected changes in 2-year and 100-year return levels (50% and 1% yearly exceedance probability, respectively) for the end of the century

(difference between ~2080-2100 and ~1980-2005) under the RCP8.5 emission scenario. (a) Distribution of the projected change and relative uncertainty (90% confidence interval considering uncertainties both in climate projections and local constraints) shown as transposed cumulative distributions; colours refer to the five groups of stations as in Fig. 1a. (b-c) Map of the projected changes for the 2-year (b) and 100-year (c) return levels.

5 Discussion and conclusions

In the south-eastern Mediterranean, the dominance of two precipitating systems and the availability of high-density local data makes it possible to simplify the statistical description of ordinary precipitation events, and therefore of extreme events that emerge as the tails of their distributions. Previous studies on the water resources of the region projected a "less rainfall, more extremes" situation, with increased extremes insufficient to impact water resources in generally drying conditions. However, these previous studies could not quantify changes in extreme return levels and therefore risk (Alpert et al., 2002; Peleg et al., 2015). Combining information on the occurrence frequency and intensity of the two dominant precipitation types from ESM projections and observational constraints from rain stations, we show that the changes in extreme return levels strictly depend on the sought probability. A tendency towards a general decrease in the intensity of the 2-year events is found, together with an increase of the most severe (100-year) events along the coast and in the desert areas.

The robustness of the synoptic variations in the RCP8.5 scenario in the region (Hochman et al., 2018a; Zappa et al., 2015) and of the local constraints (Fig. S6), demonstrate the reliability of the proposed approach and the local projected response. Nevertheless, our predictions may be refined by analysing additional scenarios and local data. It is plausible that similar improvements in the projection of extremes can be made in other regions, even though projected changes in the synoptic circulation systems might me less robust (Shepherd, 2014), calling for specific efforts to narrow this source of uncertainty. Additionally, future climate might reach some tipping point after which the observational local constraints may no longer hold, a possibility that could be tested using long simulations from convection-permitting models. For example, new synoptic systems could be introduced in the region (such as tropical-like cyclones), or the track of existing systems could change to such a degree that the interactions with local features might change substantially, thus deviating from the observed constraints (e.g. northward shift of Mediterranean cyclones track). Our results, which pertain to daily precipitation, assume no change in the spatial structure of precipitation events at scales smaller than the resolutions of the used climate models. Improvements in the statistical description of the precipitating systems at multiple temporal and spatial scales derived from observations and/or convection permitting models could fill this gap by quantifying their structural response to external forcing (Cannon and Innocenti, 2019; Wasko et al., 2016; Peleg et al., 2018; Marra et al., 2020b).

In contrast to traditional methods, the local constraints approach does not require long records; rather, it only requires local observations of ordinary events to constrain the intensity distributions. To this end, remotely sensed precipitation datasets represent a promising source of information for ungauged areas (Marra et al., 2019b). While uncertainty in ESMs remains a significant challenge to the community (Palmer and Stevens, 2019), our results point to increased investment in local measurements as an actionable and promising path to reduced uncertainty in the projection of extremes, independent of climate modelling efforts.

The framework can be extended to other processes whose extremes emerge from underlying distributions of ordinary events, such as extremes emerging from the combination of different physical phenomena, e.g. winds and storm surges from different types of cyclones (Miniussi et al., 2020; Cavicchia et al., 2020)0. Similarly, it can be applied to phenomena whose intensity and occurrence may change independently, e.g. occurrence and maximum lifetime intensity of tropical cyclones (Knutson et al., 2010). In regions where local constraints can be obtained, the approach proposed here can improve the predictability of climate change impact on extremes at scales relevant for impact studies, whose uncertainty was previously considered irreducible due to modelling uncertainty and natural variability.

Acknowledgements

The authors declare no conflict of interests. Precipitation data were provided by Israel Meteorological Service (https://ims.gov.il/en, September 2018; data is freely available in Hebrew only) and Ministry of Water and Irrigation of Jordan, Technical Affairs, Studies Directorate, Hydrological and Meteorological Information Systems (rainfall stations archives files, October 2018; available upon request to the data providers). The authors thank Prof. Pinhas Alpert for the synoptic classification. Data and codes supporting the results are available at: https://doi.org/10.5281/zenodo.4286160 and https://doi.org/10.5281/zenodo.3971558. The linear fit with uncertainty in x and y was performed based on the function by J. Browaeys, MATLAB Central File Exchange (https://www.mathworks.com/matlabcentral/fileexchange/45711-linear-fit-with-both-uncertainties-in-x-and-in-y, retrieved March 25, 2020). This study was funded by the Israel Ministry of Science and Technology [grant no. 61792], Israel Science Foundation [grant no. 1069/18], NSF-BSF [grant no. BSF 2016953], JNF [grant no. 90-01-550-18] and Google [gift grant]. It is a contribution to the HyMeX program. Authors contribution: Conceptualization: FM, MA, OA, DZ, EM; Formal analyses: FM; Data curation: FM, OG; Funding acquisition: EM, OA, CG, UD, DRE, YE; Paper writing: FM; Paper review and editing: all authors.

References

Alpert P *et al* 2002 The paradoxical increase of mediterranean extreme daily rainfall in spite of decrease in total values. *Geophys. Res. Lett.* **29(11)**, 31

Alpert P, Osetinsky I, Ziv B, Shafir H 2004 Semi-Objective Classification for Daily Synoptic Systems: Application to the Eastern Mediterranean Climate Change. *Int. J. Climatol.* **24(8)**, 1001–11

Armon M, Dente E, Smith JA, Enzel Y, Morin E 2018 Synoptic-scale control over modern rainfall and flood patterns in the levant drylands with implications for past climates. *J. Hydrometeorol.* **19**, 1077–1096

Benestad RE, Nychka D, Mearns LO 2012 Spatially and temporally consistent prediction of heavy precipitation from mean values. *Nature Clim. Change* **2**, 544-547

Blöschl G *et al* 2019 Twenty-three unsolved problems in hydrology (UPH) – a community perspective. *Hydrol. Sci. J.* **64(10)**, 1141–1158

Buishand, T.A., 1991. Extreme rainfall estimation by combining data from several sites. *Hydrol. Sci. J.*, **36 (4)**, 345–365, doi:10.1080/02626669109492511

Calinski T, Harabasz JA 1974 dendrite method for cluster analysis. *Comm. Stat.* **3(1)**, 1–27

Cannon AJ, Innocenti S 2019 Projected intensification of sub-daily and daily rainfall extremes in convection-permitting climate model simulations over North America: implications for future intensity–duration–frequency curves. *Nat. Hazards Earth Syst. Sci.* **19**, 421–440

Cavanaugh NR, Gershunov A, Panorska AK, Kozubowski TJ 2015 The probability distribution of intense daily precipitation. *Geophys. Res. Lett.* **42**, 1560–1567

Cavicchia L, Pepler A, Dowdy A, Evans J, Di Luca A, Walsh K 2020 Future changes in the occurrence of hybrid cyclones: The added value of cyclone classification for the east Australian low-pressure systems. *Geophys. Res. Lett.* **47**, e2019GL085751

Ceola S, Laio F, Montanari A 2014 Satellite Night Time Lights Reveal Increasing Human Exposure to Floods Worldwide *Geophys. Res. Lett.* **41(20)**, 7184–90

Chow VT, Maidment DR, Mays LW 1988 *Applied Hydrology*, McGraw-Hill

Coles S 2001 *An Introduction to Statistical Modeling of Extreme Values*, Springer-Verlag, London

Diskin MH 1970 Factors affecting variations of mean annual rainfall in Israel. *Int. Ass. Sci. Hydrol. Bull.* **15:4**, 41-49

Fatichi S, Ivanov VY, Paschalis A, Peleg N, Molnar P, Rimkus S, Kim J, Burlando P, Caporali E 2016 Uncertainty partition challenges the predictability of vital details of climate change. *Earth's Future* **4(5)**, 240-251

Fischer EM, Knutti R 2016 Observed heavy precipitation increase confirms theory and early models. *Nat. Clim. Change* **6**, 986-991

Fischer EM, Beyerle U, Knutti R 2013 Robust spatially aggregated projections of climate extremes. *Nat. Clim. Change* **3**, 1033–1038

Fosser, G., Kendon, E. J., Stephenson, D., & Tucker, S. (2020). Convection-permitting models offer promise of more certain extreme rainfall projections. *Geophys. Res. Lett.*, **47**, e2020GL088151

Giorgi F 2006 Climate change Hot-spots. *Geophys. Res. Lett.* **33**, L08707

Hausfather Z, Drake HF, Abbot T, Schmidt GA 2019 Evaluating the Performance of Past Climate Model Projections, *Geophys. Res. Lett.* **47**, e2019GL085378

Hochman A, Harpaz T, Saaroni H, Alpert P 2018a Synoptic classification in 21st century CMIP5 predictions over the Eastern Mediterranean with focus on cyclones. *Int. J. Climatol.* **38**, 1476-1483

Hochman A, Mercogliano P, Alpert P, Saaroni H, Bucchignani E 2018b High-resolution projection of climate change and extremity over Israel using COSMO-CLM. *Int. J. Climatol.* **38(14)**, 5095-5106

IPCC 2014 *Climate Change 2014: Synthesis Report. Contribution of Working Groups I, II and III to the Fifth Assessment Report of the Intergovernmental Panel on Climate Change*, Core Writing Team, R.K. Pachauri and L.A. Meyer eds. IPCC, Geneva, Switzerland

Keller M, Kroner N, Fuhrer O, Luthi D, Schmidli J, Stengel M, Stockli R, Schar C 2018 The sensitivity of alpine summer convection to surrogate climate change: An intercomparison between convection-parameterizing and convection-resolving models, *Atmos. Chem. Phys.* **18(8)**, 5253–5264

Kendon EJ, Roberts NM, Fowler HJ, *et al* 2014 Heavier summer downspours with climate change revealed by weather forecast resolution model. *Nat. Clim. Change.* **4**, 570-576

Knutson TR *et al* 2010 Tropical cyclones and climate change. *Nat. Geosci.* **3**, 157-163

Marani M, Ignaccolo M 2015 A metastatistical approach to rainfall extremes. *Adv. Water Resour.* **79**, 121–126

Marra F, Armon M, Borga M, Morin E 2020a Orographic effect on extreme precipitation statistics peaks at hourly time scales. Under review. *Preprint available at* doi:10.1002/essoar.10504622.1

Marra F, Borga M, Morin E 2020b A Unified Framework for Extreme Sub-daily Precipitation Frequency Analyses based on Ordinary Events. *Geophys. Res. Lett.*, **47**, e2020GL090209

Marra F, Nikolopoulos EI, Anagnostou EN, Bárdossy A, Morin E 2019b Precipitation frequency analysis from remotely sensed datasets: A focused review. *J. Hydrol.* **574**, 699-705

Marra F, Nikolopoulos EI, Anagnostou EN, Morin E 2018 Metastatistical Extreme Value analysis of hourly rainfall from short records: Estimation of high quantiles and impact of measurement errors. *Adv. Water Resour.* **117**, 27-39

Marra F, Zoccatelli D, Armon M, Morin E 2019a A simplified MEV formulation to model extremes emerging from multiple nonstationary underlying processes. *Adv. Water Resour.* **127**, 280-290

Miniussi A, Villarini G, Marani M 2020 Analyses through the Metastatistical Extreme Value distribution identify contributions of Tropical Cyclones to rainfall extremes in the Eastern US. *Geophys. Res. Lett.* **47**, e2020GL087238

Myhre G *et al* 2019 Frequency of extreme precipitation increases extensively with event rareness under global warming. *Sci. Reports* **9**, 16063

NOAA, 2020 U.S. billion-dollar weather and climate disasters. NCEI, https://www.ncdc.noaa.gov/billions/summary-stats

O'Gorman PA, Schneider T 2009 The physical basis for increases in precipitation extremes in simulations of 21st-century climate change. *Proc. Natl. Acad. Sci. U. S. A.*, **106(35)**, 14773-14777

Overeem A, Buishand A, Holleman I 2008 Rainfall depth-duration-frequency curves and their uncertainties. *J. Hydrol.* **348**, 124–134

Palmer T, Stevens B 2019 The scientific challenge of understanding and estimating climate change. *Proc. Natl. Acad. Sci. U. S. A.* **116(49)**, 24390-24395

Papalexiou SM, AghaKouchak A, Foufoula-Georgiou E 2018 A diagnostic framework for understanding climatology of tails of hourly precipitation extremes in the United States. *Water Resour. Res.* **54**, 6725–6738

Paprotny D, Sebastian A, Morales-Napoles O, Jonkman SN 2018 Trends in flood losses in Europe over the past 150 years. *Nat. Comm.* **9**, 1985

Peleg N, Marra F, Fatichi S, Molnar P, Morin E, Sharma A, Burlando P 2018 Intensification of convective rain cells at warmer temperatures observed from high-resolution weather radar data. *J. Hydrometeorol.* **19**, 715-726

Peleg N, Shamir E, Georgakakos KP, Morin E 2015 A framework for assessing hydrological regime sensitivity to climate change in a convective rainfall environment: a case study of two medium-sized eastern Mediterranean catchments, Israel *Hydrol. Earth Syst. Sci.* **19**, 567–581

Pendergrass AG 2018 What precipitation is extreme? *Science* **360**, 6393

Pendergrass AG, Knutti R 2018 The uneven nature of daily precipitation and its change. *Geophys. Res. Lett.* **45**, 11980–11988

Pfahl S, O'Gorman PA, Fischer EM 2017 Understanding the regional patter of projected future changes in extreme precipitation. *Nat. Clim. Change* **7**, 423-428

Phillips P, Perron P 1988 Testing for a Unit Root in Time Series Regression. *Biometrika* **75**, 335–346

Riahi K, Rao S, Krey V, Cho C, Chirkov V, Fischer G, Kindermann G, Nakicenovic N, Rafaj P 2011 RCP 8.5 – A scenario of comparatively high greenhouse gas emissions. *Clim. Change* **109**, 33-57

Rinat Y, Marra F, Armon M, Metzger A, Levi Y, Khain P, Vadislavsky E, Rosensaft M, Morin E 2020 Hydrometeorological analysis and forecasting of a 3-day flash-flood-triggering desert rainstorm, *Nat. Hazards Earth Syst. Sci. Discuss.*, Under review, Preprint available at doi:10.5194/nhess-2020-189

Samuels R, Rimmer A, Alpert P 2009 Effect of extreme rainfall events on the water resources of the Jordan River. *J. Hydrol.* **375**, 513-523

Schär C *et al* 2016 Percentile indices for assessing changes in heavy precipitation events. *Clim. Change* **137**, 201-216

Serinaldi F, Kilsby CG 2015 Stationarity is undead: Uncertainty dominates the distribution of extremes. *Adv. Water Resour.* **77**, 17-36

Shepherd TG 2014 Atmospheric circulation as a source of uncertainty in climate change projections. *Nat. Geosci.* **7**, 703–708

Shmilovitz Y, Morin E, Rinat Y, Haviv I, Carmi G, Mushkin A, Enzel Y 2020 Linking frequency of rainstorms, runoff generation and sediment transport across hyperarid talus-pediment slopes. *Earth Surf. Proc. Landforms* **49(7)**, 1644-1659

Sippel S, Mitchell D, Black MT, Dittus AJ, Harrington L, Schaller N, Otto FEL 2015 Combining large model ensembles with extreme value statistics to improve attribution statements of rare events. *Weather Clim. Extremes* **9**, 25-35

Wasko C, Lu WT, Mehrotra R 2018 Relationship of extreme precipitation, dry-bulb temperature, and dew point temperature across Australia. *Env. Res. Lett.* **13**, 074031

Wasko C, Sharma A, Westra S 2016 Reduced spatial extent of extreme storms at higher temperatures. *Geophys. Res. Lett.* **43**, 4026–4032

Wilcox EM, Donner LJ 2007 The frequency of extreme rain events in satellite rain-rate estimates and an atmospheric general circulation model. *J. Climate* **20**, 53–69

Winsemius HC *et al* 2016 Global drivers of future river flood risk. *Nat. Clim. Change* **6**, 381-385

Zappa G, Hawcroft MK, Shaffrey L, Black E, Brayshaw DJ 2015 Extratropical cyclones and the projected decline of winter Mediterranean precipitation in the CMIP5 models. *Clim. Dyn.* **45(7–8)**, 1727–1738

Zorzetto E, Botter G, Marani M 2016 On the emergence of rain- fall extremes from ordinary events. *Geophys. Res. Lett.* **43**, 8076–8082

Geophysical Research Letters

Supporting Information for

Towards narrowing uncertainty in future projections of local extreme precipitation

Francesco Marra[1,2,*], Moshe Armon[1], Ori Adam[1], Davide Zoccatelli[1], Osama Gazal[3], Chaim I. Garfinkel[1], Dorita Rostkier-Edelstein[1,4], Uri Dayan[5], Yehouda Enzel[1], and Efrat Morin[1]

[1]The Fredy and Nadine Herrmann Institute of Earth Sciences, The Hebrew University of Jerusalem, Israel

[2]Institute of Atmospheric Sciences and Climate, National Research Council of Italy, CNR-ISAC, Bologna, Italy

[3]Faculty of Agricultural and Environmental Sciences, Szent Istvan University, Hungary

[4]Department of Environmental Physics, Environmental Sciences Division, IIBR, Ness-Ziona, Israel

[5]Department of Geography, The Hebrew University of Jerusalem, Israel

Contents of this file

Code	Alpert et al. (2004)	Precipitation type in this study
1	Red Sea Trough with the Eastern axis	2
2	Red Sea Trough with the Western axis	2
3	Red Sea Trough with the Central axis	2
4	Persian Trough (Weak)	3
5	Persian Trough (Medium)	3
6	Persian Trough (Deep)	3
7	High to the East	3
8	High to the West	3
9	High to the North	3
10	High over Israel (Central)	3
11	Low to the East (Deep)	1
12	Cyprus Low to the South (Deep)	1
13	Cyprus Low to the South (Shallow)	1
14	Cyprus Low to the North (Deep)	1
15	Cyprus Low to the North (Shallow)	1
16	cold Low to the West	1
17	Low to the East (Shallow)	1
18	Sharav Low to the West	2
19	Sharav Low over Israel (Central)	2

Table S1. Synoptic systems in the semi-automatic classification by Alpert at al. (2004) and corresponding precipitation types used in this study, as follows: (1) *Type-1* (Mediterranean cyclones), (2) *Type-2* (other type of systems), (3) individually examined and labelled as *Type-1* if occurring up to 2 days after a *Type-1* wet day, and as *Type-2* in the remaining cases

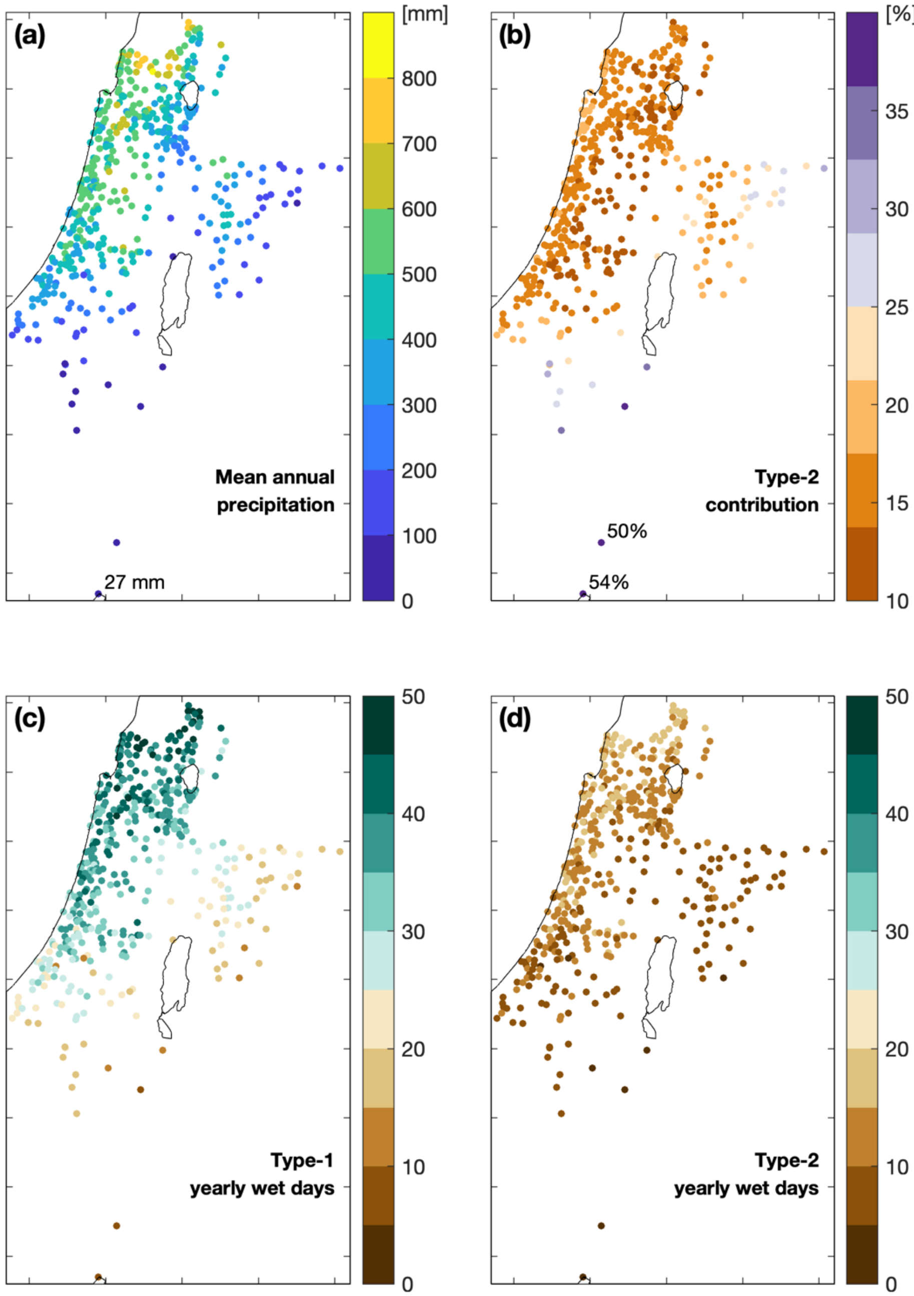

Figure S1. Mean annual precipitation. (a) Mean annual precipitation in the south-eastern Mediterranean. Precipitation is mainly contributed by Mediterranean cyclones (*Type-1*) as shown in the other panels. (b) Relative contribution to the mean annual precipitation from *Type-2* events. Average yearly number of *Type-1* (c) and *Type-2* (d) wet days.

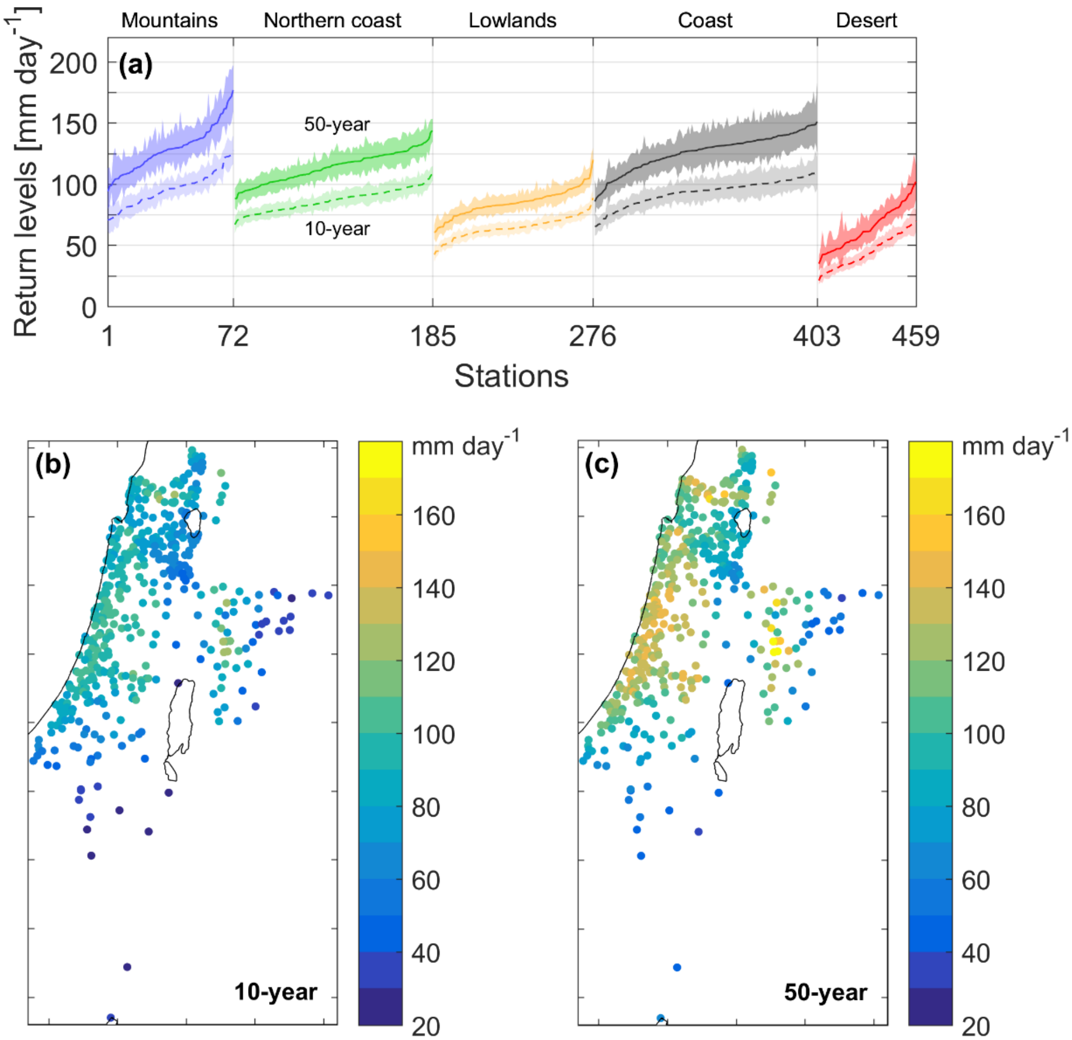

Figure S2. (a) Distribution of return levels and relative uncertainty (90% confidence interval from 103 bootstrap samples with replacement among the years in the record) shown as transposed cumulative distributions; colors refer to for the five groups of stations in Fig. 1a. (b, c) Map of the 10-year (c) and 50-year (d) return levels (10% and 2% yearly exceedance probability).

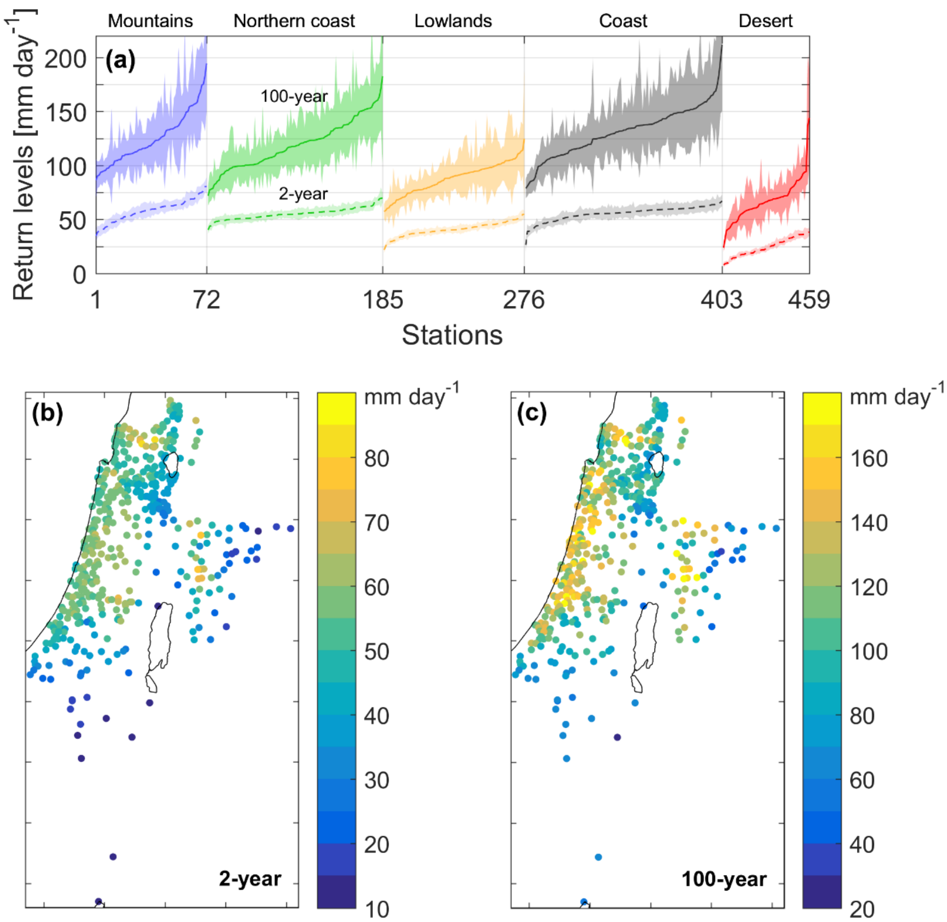

Figure S3. Extreme return levels computed using traditional approaches. Two-year and 100-year return levels (50% and 1% yearly exceedance probability) for daily precipitation amounts computed using traditional methods based on extreme value theory: a Generalized Extreme Value distribution is fitted to the annual maxima series using the method of the L-moments (Hosking, 1990). (a) Distribution of return levels and relative uncertainty (90% confidence interval from 103 bootstrap samples with replacement among the years in the record) shown as transposed cumulative distributions; median uncertainty of 17% (39%) for 2-year (100-year) return levels. The colors of the five groups of stations are as in Fig. 1a. (b, c) Map of the 2-year (c) and 100-year (d) return levels (50% and 1% yearly exceedance probability). Note the larger spatial variability (noise) of the return levels relative to Fig. 1, reflecting the largely increased uncertainty characterizing traditional methods based on the analysis of observed extremes (here, the annual maxima).

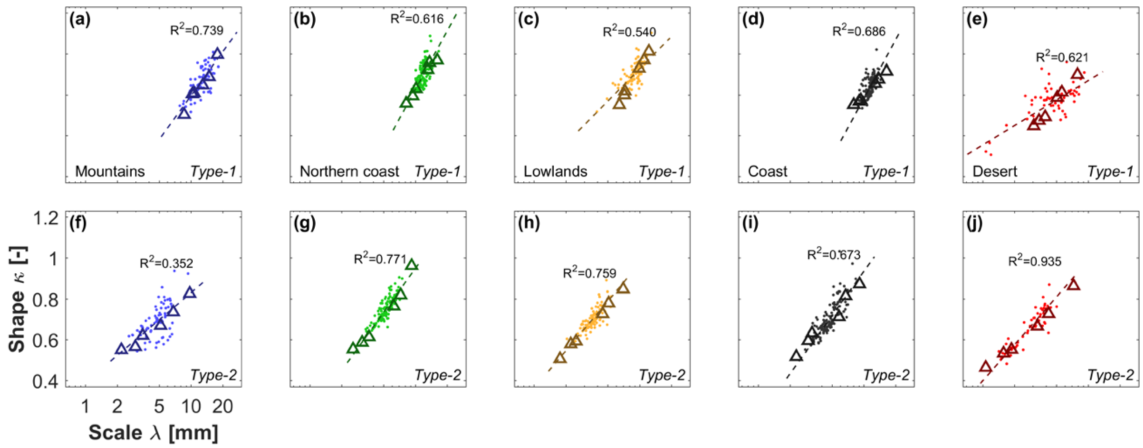

Figure S4. Local constraints of the parameters of the intensity distribution of the ordinary events. Scatter plot of the scale (λ) and shape (κ) parameters of the observed Weibull distributions for the two types of ordinary events and for the five groups of stations; colors as in Fig. 1a. The regressions used to define the local constraints (α coefficients) are shown as dashed lines. Triangles represent the median (among stations) parameters obtained using, for each station, groups of five non-consecutive years with increasing median intensity of the ordinary events.

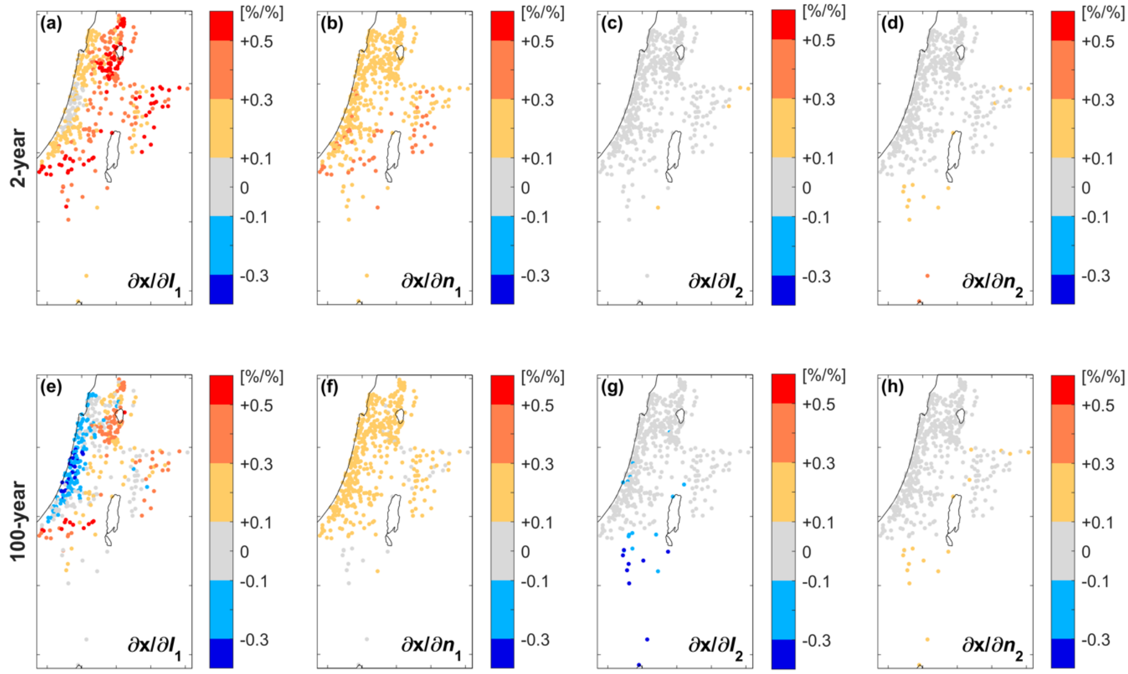

Figure S5. Sensitivity of extreme return levels to changes in the average characteristics of ordinary events. Sensitivity of 2-year (a-d) and 100-year (e-h) return levels (50% and 1% yearly exceedance probability) to changes in median intensity (I) and expected number of yearly occurrence (n) of the two types of ordinary events. The sensitivity or extreme return levels $x(p)$ to changes in the median intensity and in the expected number of ordinary events is computed numerically using the partial derivatives of $x(p) = \zeta^{(-1)}(p; I_1, n_1; I_2, n_2)$ with respect to the four variables, i.e., $\frac{\partial x(p)}{\partial I_1}$, $\frac{\partial x(p)}{\partial I_2}$, $\frac{\partial x(p)}{\partial n_1}$, and $\frac{\partial x(p)}{\partial n_2}$. Units of change in x per 1% change in the predictor are quantified. The figure highlights two important points. First, different return levels can have different responses. Since practical applications rely on different return levels, this implies that the potential impact of climate change strongly depends on the application of interest. For instance, sewer systems are generally designed to be overtopped not more than once in 2-5 years. In contrast, dams, bridges and river dikes are designed for much lower probabilities of failure (e.g., 100- or even 1000-year). Second, the local sensitivities associated with each type of event can differ significantly. Therefore, local changes in extremes are related to mean (or median) changes in precipitation in a complex manner.

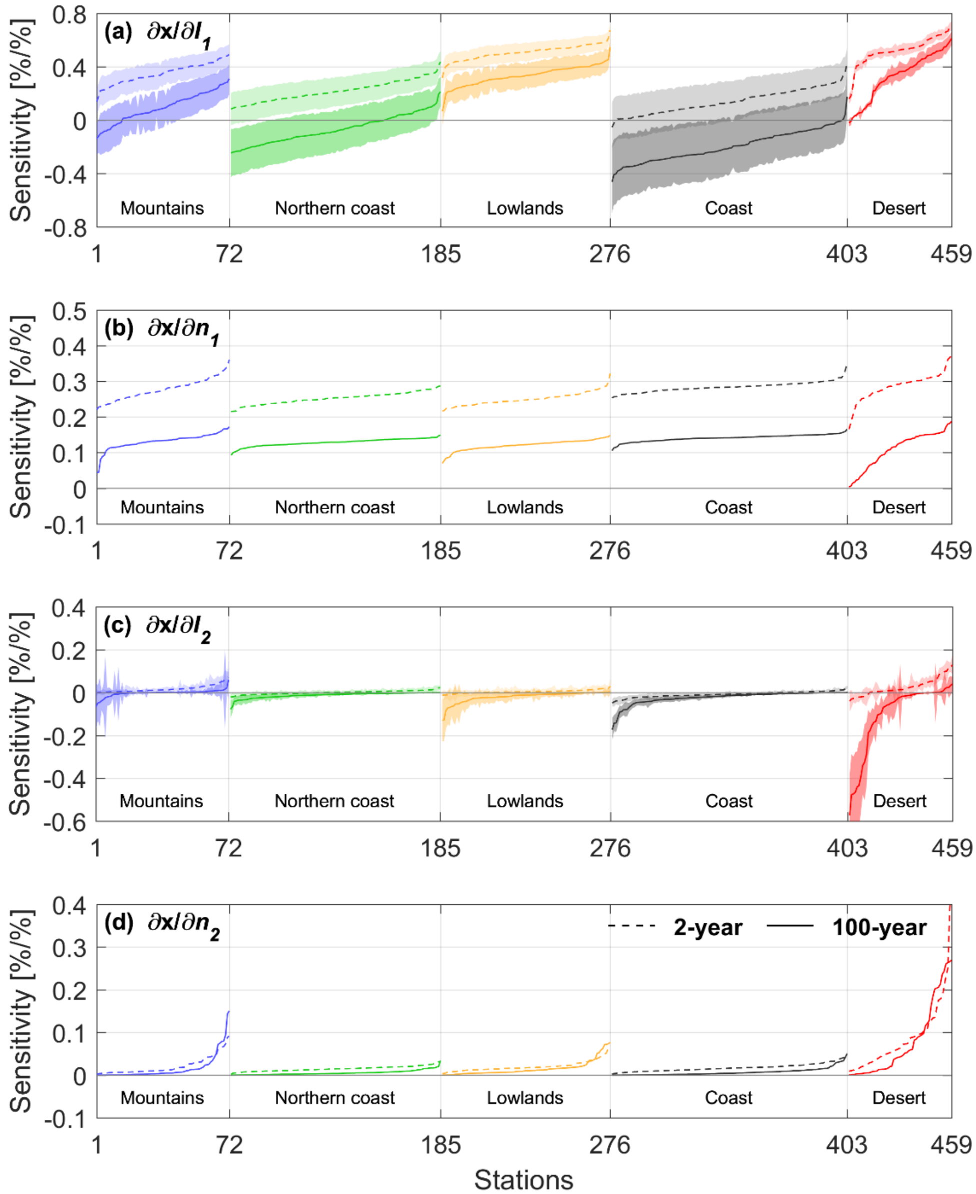

Figure S6. Sensitivity of extreme return levels to changes in the ordinary events. Distribution of the sensitivity of 2-year and 100-year return levels to changes in the average characteristics of the two types ordinary events shown as transposed cumulative distributions; uncertainties in the sensitivity to the median intensities are computed as 90% confidence interval of the local constrains (90% confidence interval of the α coefficients). (a) Sensitivity to the *Type-1* intensity. (b) Sensitivity to the *Type-1* yearly number of events. (c) Sensitivity to the *Type-2* intensity. (d) Sensitivity to the *Type-2* yearly number of events.

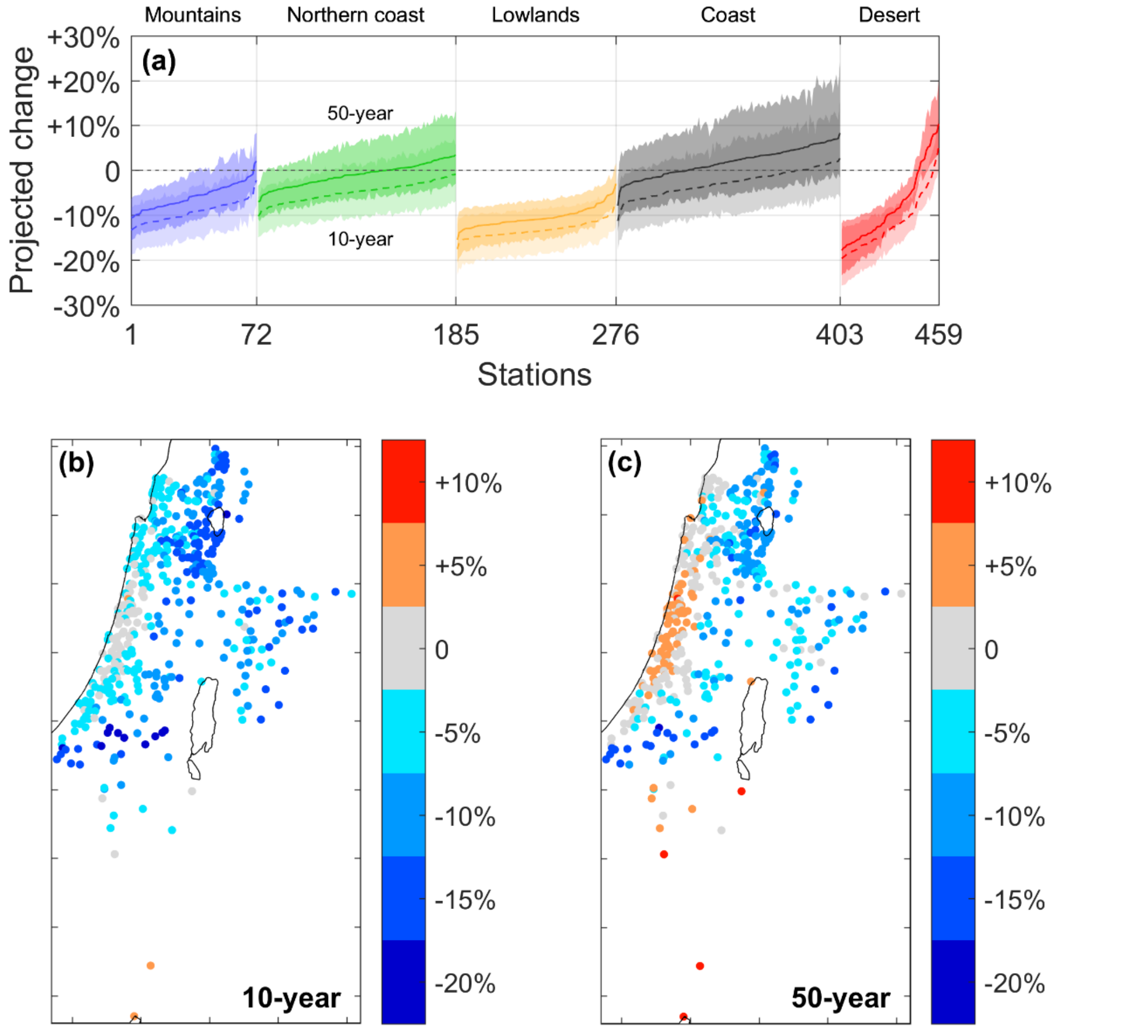

Figure S7. Projected changes in extreme precipitation return levels (RCP8.5 emission scenario; 10-year and 50-year return levels). Projected changes in 10-year and 50-year return levels (10% and 2% yearly exceedance probability) for the end of the century (difference between ~2080-2100 and ~1980-2005) under the RCP8.5 emission scenario. (a) Distribution of the projected change and relative uncertainty (90% confidence interval considering uncertainties in climate projections and local constraints) shown as transposed cumulative distributions; colors as in Fig. 1a. (b-c) Map of the projected change for the 10-year (b) and 50-year (c) return levels.

References

Alpert P, Osetinsky I, Ziv B, Shafir H 2004 Semi-Objective Classification for Daily Synoptic Systems: Application to the Eastern Mediterranean Climate Change. Int. J. Climatol. 24(8), 1001–11

Hosking JRM 1990 L-moments: Analysis and estimation of distributions using linear combinations of order statistics. J. Royal Stat. Soc. B, 52(1), 105–124